

# Recoiling from a kick in the head-on collision of spinning black holes

Dae-Il Choi,<sup>1,2</sup> Bernard J. Kelly,<sup>1</sup> William D. Boggs,<sup>3</sup> John G. Baker,<sup>1</sup> Joan Centrella,<sup>1</sup> and James van Meter<sup>1</sup>

<sup>1</sup>*Gravitational Astrophysics Laboratory, NASA Goddard Space Flight Center, 8800 Greenbelt Rd., Greenbelt, MD 20771, USA*

<sup>2</sup>*Korea Institute of Science and Technology Information,*

*52-11, Eoun-Dong, Yuseong-Gu, Daejeon, South Korea, 305-806*

<sup>3</sup>*University of Maryland, Department of Physics, College Park, MD 20742, USA*

(Dated: August 8, 2018)

Recoil “kicks” induced by gravitational radiation are expected in the inspiral and merger of black holes. Recently the numerical relativity community has begun to measure the significant kicks found when both unequal masses and spins are considered. Because understanding the cause and magnitude of each component of this kick may be complicated in inspiral simulations, we consider these effects in the context of a simple test problem. We study recoils from collisions of binaries with initially head-on trajectories, starting with the simplest case of equal masses with no spin and then adding spin and varying the mass ratio, both separately and jointly. We find spin-induced recoils to be significant relative to unequal-mass recoils even in head-on configurations. Additionally, it appears that the scaling of transverse kicks with spins is consistent with post-Newtonian theory, even though the kick is generated in the nonlinear merger interaction, where post-Newtonian theory should not apply. This suggests that a simple heuristic description might be effective in the estimation of spin-kicks.

PACS numbers: 04.25.Dm, 04.25.Nx, 04.30.Db, 04.70.Bw, 95.30.Sf, 97.60.Lf

## I. INTRODUCTION

The coalescence of spinning black holes in a binary system is expected to occur throughout the universe, on scales ranging from stellar black holes formed as the end-products of stellar evolution to supermassive black holes that lurk at the centers of galaxies. The final merger of such systems will produce an intense burst of gravitational radiation; if this radiation is emitted asymmetrically, as in the case of unequal masses and spins, the resulting remnant black hole will experience a recoil kick. The magnitude of this kick is important in a variety of astrophysical situations, such as the cosmological evolution of supermassive black holes [1, 2, 3, 4, 5, 6, 7, 8] and the growth and retention of intermediate-mass black holes in dense stellar clusters [9, 10, 11, 12, 13, 14, 15], and it also affects the expected rates of black hole mergers for gravitational wave detectors [16]. Given the importance of recoil kicks in astrophysics, there have been numerous analytic studies of this phenomenon [17, 18, 19, 20, 21, 22, 23, 24, 25]. However, since nearly all of the recoil occurs in the regime of strong gravitational fields, numerical relativity simulations are essential to obtain accurate calculations of the kick.

Recent breakthroughs in binary black hole simulations [26, 27, 28, 29] now allow extensive studies of equal mass nonspinning black hole mergers [30, 31, 32]. Calculations of the kick resulting from mergers of nonspinning black holes with unequal masses have been carried out for mass ratios  $q = m_1/m_2$  in the range  $q = 1$  to  $q = 0.25$  [33, 34, 35], with the maximum kick velocity estimated to be  $\sim 175\text{km/s}$  for mass ratio  $q \sim 0.36$  [35]. In addition, several simulations of mergers of equal mass, spinning

black holes have been carried out [36, 37, 38].

Most recently, several papers have appeared that address the kicks obtained from the inspiral of spinning binaries of equal [39, 40] and unequal masses [41]. These papers find considerable kicks resulting from the addition of symmetry-breaking spins perpendicular to the orbital plane, leading to a total kick speed of  $\sim 440\text{km/s}$ . Moving to spins initially in the orbital plane, [42] suggested a “superkick” orbital configuration; this was investigated by Gonzalez *et al.* [43], who found an associated kick of  $\sim 2500\text{km/s}$ . Extrapolated to maximally spinning pre-merger holes, this may lead to a kick as high as  $\sim 4000\text{km/s}$  [42].

Nevertheless the complexity of the binary orbital evolution may obscure details such as the direction of the final kick, and its dependence on mass ratio and spin. With this in mind, we present here a study of a simpler problem, which may be seen as an approximation to the final plunge to merger. We chose the head-on case as a model problem to isolate kick effects from the orbital inspiral motion. Although lacking in astrophysical likelihood, our head-on investigations have the advantage of removing directional ambiguity in the kicks produced. In particular, we can readily test the leading-order post-Newtonian (PN) prediction that the spin and mass-ratio contributions to the kick should be orthogonal.

In our investigation of the recoil kicks produced by the merger of spinning black holes in head-on collisions, we vary both the black hole spins and mass ratio. We find definite transverse kicks from the merger of equal-mass holes with spin. Furthermore, the total kick momentum imparted appears to scale roughly with the sum of the black hole spin parameters,  $a_1 + a_2$ . For the cases investigated, these kicks yield transverse kick velocities in the

range  $\sim 15 - 30\text{km/s}$ . We have also seen longitudinal (along the line of motion of the holes) kicks, due to a non-unity mass ratio. These kicks are much more modest in magnitude, with velocities of  $\sim (2-5)\text{km/s}$  for the mild mass ratio  $q = 2/3$  chosen.

This work is carried out using the moving puncture method [27, 28, 44, 45, 46, 47]. We describe our initial data in Sec. II and our numerical methodology in Sec. III. Code calibration and testing is presented in Sec. IV. We present our results in Sec. V and conclude with a discussion in Sec. VI.

## II. INITIAL DATA

We set up initial data for binary black holes represented as “punctures” [48]. The metric on the initial spacelike slice is written in the form  $g_{ij} = \psi^4 \delta_{ij}$ , where  $i, j = 1, 2, 3$ , with conformal factor  $\psi = \psi_{\text{BL}} + u$ . The singular part of the conformal factor takes the form  $\psi_{\text{BL}} = 1 + \sum_{A=1}^2 m_{A,p}/2|\vec{r} - \vec{r}_A|$ , where the  $A^{\text{th}}$  black hole has mass parameter (or “puncture mass”)  $m_{A,p}$  and is located at coordinate position  $\vec{r}_A$ . The nonsingular function  $u$  is calculated by solving the Hamiltonian constraint equation using the second-order-convergent elliptic solver AMRMG [49].

The black holes start out at rest. We use the Bowen-York (BY) [50] form of the extrinsic curvature to incorporate black hole spin:

$$K_{A,ij}^S = \psi^{-2} \frac{3}{r_A^3} [\epsilon_{kim} S_A^m n_A^k n_{Aj} + \epsilon_{kjm} S_A^m n_A^k n_{Ai}], \quad (1)$$

where  $\vec{n}_A$  is the unit vector in the direction of increasing  $r_A$  and  $\vec{S}_A$  is the spin angular momentum of the  $A^{\text{th}}$  black hole. In all cases we take  $\vec{S}_A$  to be aligned with the  $z$  axis, so that  $\vec{S}_A = S_A \hat{e}_z$ .

In all, we consider head-on collisions for seven different initial configurations of both equal (EQ) and unequal (NE) masses, and varied spins. The initial directly specified parameters of all the simulations are listed in Table I, while derived quantities are given in Table II; all length scales are given in terms of a fiducial mass  $M$  [which coincides with the Arnowitt-Deser-Misner (ADM) mass of the system for equal-mass runs]. For each run, the punctures were initially placed on the  $y$  axis with the center of mass at the origin. The proper separation  $l$  between the holes, along the initial slice, is measured between the closest parts of the apparent horizons along the  $y$  axis. We note that  $l$  is not necessarily the smallest physical distance between the holes (in this spatial slice), as spin effects can twist the space-like geodesics off the coordinate axis.

We use the *horizon mass*  $m$  to define the black hole mass ratio  $q$  on the initial slice,

$$q = m_1/m_2, \quad (2)$$

TABLE I: Directly specified parameters of the numerical simulations, in terms of the fiducial mass  $M$ .  $S_A^z$  is the non-zero component of the Bowen-York angular momentum on each hole. NEa $_{+-}$  and NEb $_{+-}$  are, respectively, large-separation and equal-spin-parameter variants of NE $_{+-}$ , as explained in the text.

Run	$m_{1,p}/M$	$m_{2,p}/M$	$y_1/M$	$y_2/M$	$S_1^z/M^2$	$S_2^z/M^2$
EQ $_{00}$	0.5000	0.5000	4.0	-4.0	0.0	0.0
NE $_{00}$	0.4909	0.7478	4.8348	-3.2232	0.0	0.0
EQ $_{+0}$	0.3444	0.5000	4.0	-4.0	0.2	0.0
EQ $_{+-}$	0.3444	0.3444	4.0	-4.0	0.2	-0.2
NE $_{+-}$	0.3436	0.7140	4.8	-3.2	0.2	-0.2
NEa $_{+-}$	0.3436	0.7140	7.2	-4.8	0.2	-0.2
NEb $_{+-}$	0.3436	0.5496	4.8	-3.2	0.2	-0.4486

where  $m_1$  is the horizon mass of the lighter hole. The symmetric mass ratio is

$$\nu \equiv m_1 m_2 / (m_1 + m_2)^2. \quad (3)$$

The horizon mass is derived from the apparent horizon’s *irreducible mass* using the Christodoulou formula [52]:

$$m^2 = m_{irr}^2 + \frac{S^2}{4m_{irr}^2}, \quad (4)$$

where  $m_{irr} = \sqrt{A_{AH}/16\pi}$  and  $A_{AH}$  is the area of the apparent horizon, which we locate using an adapted version of Jonathan Thornburg’s `AHFinderDirect` code [53].

The spin vector  $\vec{S}$  applied to each hole in the Bowen-York data prescription (1) is in fact the ADM angular momentum of that hole – the total angular momentum of the spatial slice as measured by an ADM integral at infinity if no other sources were present. Thus these parameters represent a global quantity.

The more standard definition of astrophysical black-hole spin, however, is a local one. The Kerr solution is parametrized by the black hole horizon mass  $m$ , and a spin parameter  $a$  restricted to the range of values  $[0, m]$ . Then,  $a = |\vec{S}|/m$ . We note, however, that it has proved impossible to bring Bowen-York spinning data to an  $a$  value of more than  $\sim 0.927m$ , significantly below the maximal Kerr value [54].

Even in the head-on case, with spin vectors orthogonal to the separation vector, there is much freedom in the parameters describing the initial data. In particular, we have chosen to scale all distances so that the horizon mass of the lighter hole,  $m_1$ , is kept the same relative to the grid spacing (ensuring a common level of resolution of that hole’s features). Within this restriction, we have also striven to maintain the same proper horizon-to-horizon separation  $l$  between the holes.

### III. METHODOLOGY

These initial data sets were evolved using the moving puncture method as implemented in the `Hahndol` code [32]. We used standard Baumgarte-Shapiro-Shibata-Nakamura (BSSN) [55, 56] evolution equations, with the addition of dissipation terms as in [57] and constraint-damping terms as in [58], in order to ensure robust stability. Our gauge conditions are 1+log lapse slicing and a hyperbolic Gamma-driver shift condition, as used in [44]. Here we take  $\eta = 2.0$ , and the initial lapse shape chosen is  $\alpha_{init} = \psi_0^{-4}$ , where  $\psi_0$  is the initial conformal factor; this gives a steeper fall-off near the punctures than the  $\psi_0^{-2}$  used in the evolutions of [32]. Time integration was carried out with a fourth-order Runge-Kutta algorithm, and spatial derivatives with fourth-order-accurate finite differencing stencils. We employed a second-order-accurate Sommerfeld condition on the outer boundary at  $256M$ ; physical modes propagating in from the outer boundary will then take  $\sim 190M$  to reach the outermost extraction sphere at  $60M$ , while gauge modes propagating at  $\sqrt{2}$  times the speed of light will take  $\sim 140M$  to reach this same sphere. As will be seen, the bulk of the merger radiation and associated momentum flux will have passed through the extraction sphere by this time. We used adaptive mesh refinement (AMR) implemented via the software package `PARAMESH` [59, 60, 61, 62], with fifth-order-accurate interpolation between refinement regions (as preservation of fourth-order accuracy in the bulk demands better than fourth-order-accurate interpolation at refinement interfaces [46, 63, 64]).

The momentum kick of the merged black hole is calculated as the aggregated time-integral of the momentum flux, or *thrust*,  $dP^i/dt$  – a surface integral of the squared time-derivative of the radiative Weyl scalar  $\psi_4$  times the unit radial vector [65]:

$$\frac{dP^i}{dt} = \lim_{R \rightarrow \infty} \left\{ \frac{R^2}{4\pi} \oint d\Omega \frac{x^i}{R} \left| \int_{t_0}^t dt' \dot{\psi}_4 \right|^2 \right\} \quad (5)$$

$$\Delta P^i = \int_{t_0}^t dt \frac{dP^i}{dt}, \quad (6)$$

where  $t_0$  is the initial time in the simulation (all time integrals above should properly be from  $t' = -\infty$ ; our implementation neglects thrust contributions from before  $t_0$ ). In fact, for reasons discussed in the next section, we must delay the integration start time  $t_0$  to when the thrust passes through zero. As (5) is quadratic in the waveform  $\psi_4$ , the kick can be expected to be weak. To perform the angular integration in (5), we use the second-order Misner algorithm described in [66, 67].

### IV. CODE CALIBRATION

We have established the convergence of the `Hahndol` code in prior publications [32, 34]. To these previously published results, we have added only one qualitatively new aspect: spin on the pre-merger holes. Thus we restrict our discussion of convergence here to a study of the convergence properties of a sample spinning data set with equal masses and anti-aligned spins,  $\text{EQ}_{+-}$ .

Our main evolutions were performed at a maximum resolution of  $M/32$  in the vicinity of the pre-merger holes. We emphasize here that, as we have maintained a smaller horizon mass of  $m \approx 0.5M$  in all runs, the grid spacing realized near the smaller hole will always be close to  $m/16$ . This yields corresponding grid spacings of  $h = M$ ,  $h = 2M$  and  $h = 8M$  at the extraction surfaces  $R_{\text{ext}} = 30M$ ,  $R_{\text{ext}} = 60M$  and the outer boundary, respectively. Relative to this standard resolution ( $M/32$ ), we have added two higher resolutions ( $M/40$  and  $M/48$ ).

Fig. 1 indicates the rate of convergence of the Hamiltonian and momentum constraints in two regions of interest: the strong-field region surrounding the holes (left panels), and the refinement level containing our  $R_{\text{ext}} = 60M$  wave-extraction sphere (right panels). In our simulations, the Hamiltonian constraint exhibits greater than third-order convergence, and the momentum constraint exhibits second-order convergence through most of the duration of the runs. This may be partly due to our second-order-accurate initial data solver; however errors of lower-than-expected order have also been attributed to “leakage” from the punctures [38, 68]. At late times the apparent convergence of the momentum constraint drops to a rate between first and second order; we believe this is because of a high-frequency gauge pulse propagating outward until it is insufficiently resolved at the grid resolution achieved in the outer zones of our coarser run. However, this gauge pulse does not significantly affect the thrust computation, as evidenced by the invariance with extraction radii demonstrated in Sec. V.

In Fig. 2, we illustrate the convergence of the dominant (2,2) mode of the Weyl scalar  $\text{Re}(\psi_4)$ , extracted at  $R_{\text{ext}} = 60M$ . For comparisons, we have lined up the main amplitude peak in time across resolutions, and rotated the waveform phase to zero at this point (similar to the *maquillage* used in inspiral waveform comparisons [31]). Resolution-dependent errors are higher during the unphysical high-frequency Bowen-York pulse (see next section); by  $\sim 100M$ , when the physical merger radiation reaches the detector, errors are consistent in overall magnitude with second-order convergence, and compare favorably with the equivalent plots in Fig. 3 of [30].

TABLE II: Derived initial parameters in terms of the fiducial mass  $M$ .  $m_1$  is the horizon mass of the lighter hole.  $q$  is the mass ratio defined by horizon masses.  $a_A = |S_A|/m_A$  is the approximate Kerr spin parameter of hole  $A$ .  $l$  is the proper horizon-horizon separation of the holes.  $M_{ADM}$  was calculated at a finite coordinate distance from the origin ( $60M$  for all but run EQ<sub>+0</sub>), using Eq. (12) of [51]. Errors in horizon masses  $m_1$  and  $m_2$  are  $\sim 1.5\%$  (see text), which propagate into derived quantities  $q$ ,  $\nu$ ,  $a_1$ ,  $a_2$ ,  $a_1/m_1$ , and  $a_2/m_2$ . ADM mass errors enter at the fourth significant digit.

Run	$m_1/M$	$m_2/M$	$q$	$\nu$	$a_1$	$a_2$	$a_1/m_1$	$a_2/m_2$	$l/M$	$M_{ADM}/M$
EQ <sub>00</sub>	0.514	0.514	1.0	0.250	0.0	0.0	0.0	0.0	12.24	1.0
NE <sub>00</sub>	0.514	0.771	0.667	0.240	0.0	0.0	0.0	0.0	12.24	1.24
EQ <sub>+0</sub>	0.516	0.514	1.004	0.250	0.389	0.0	0.758	0.0	12.24	1.0
EQ <sub>+−</sub>	0.514	0.514	1.0	0.250	0.389	0.389	0.758	0.758	$12.4 \pm 0.2$	1.0
NE <sub>+−</sub>	0.516	0.773	0.668	0.240	0.388	0.259	0.752	0.335	$12.6 \pm 0.2$	1.24
NEa <sub>+−</sub>	0.513	0.764	0.672	0.240	0.390	0.262	0.759	0.342	$17.0 \pm 0.2$	1.25
NEb <sub>+−</sub>	0.516	0.784	0.658	0.239	0.388	0.572	0.752	0.730	$13.0 \pm 0.2$	1.26

In Fig. 3, we illustrate the convergence of the momentum thrust for our data set EQ<sub>+−</sub>, extracted at  $R_{\text{ext}} = 60M$  (as for Fig. 2), beginning at the integration start time  $t_0 = 90.5M$ . To compare the different data sets, we re-zero and rescale the time axis to overlay the two largest physical peaks for all three resolutions. The differences have again been scaled for first- and second-order convergence. The thrust displays better than second-order convergence for most of the physical thrust, but has a significant excursion around  $t = 102M$ . Nevertheless, the relative errors in the thrust are  $\sim 1\%$  (compare with upper panel).

### A. Bowen-York Radiation Pulses

Bowen-York black hole initial data contains a non-negligible amount of “false radiation,” even after the Hamiltonian constraint has been solved. This radiation is unphysical in the sense that it is a reflection of the unphysical approximations, such as conformal flatness, made in generating the initial data (*c.f.* [69]).

To estimate the approximate duration of this unphysical radiation pulse, we assume that each hole relaxes to a Kerr hole (of approximately the same mass and spin) through the emission of quasinormal modes (QNMs). The most slowly damped of these will have an “e-folding” time  $\tau_e \approx 12m$  for a hole of mass  $m$  [70]. Then a pulse will have decayed by two orders of magnitude after  $\sim 55m$  – that is,  $\sim 30M$  for our equal-mass (EQ) data sets, and  $\sim 45M$  for our unequal-mass (NE) data.

This Bowen-York “pulse” is concentrated close to each hole’s horizon, and much of it falls into its parent hole, resulting in an increase in apparent-horizon mass of  $\sim 1\%$ ; however, what radiation escapes to our detection spheres

will mix with the physical radiation we are generally interested in. Nevertheless, since the pulse is released immediately, and is of short duration, it should be easily identifiable in the total waveform.

To illustrate, we show in Fig. 4 the dominant ( $l = 2, m = 2$ ) spin-2-weighted spherical harmonic mode of the “outgoing” Weyl scalar  $\psi_4$  (extracted at  $R_{\text{ext}} = 30M$ ), for three different equal-mass configurations: zero-spin (EQ<sub>00</sub>), single-spin (EQ<sub>+0</sub>) and double-spin (EQ<sub>+−</sub>). Despite the differences in spins, these three waveforms agree well in the later “physical” part of the signal, with stronger differences occurring in the non-physical BY pulse. In the zero-spin case, the BY pulse is small, but it is significant for EQ<sub>+0</sub> and EQ<sub>+−</sub>.

This same pulse will yield a non-zero contribution to the momentum kick. Again, this should be easy to identify, as it will result in a plateau early in the run. Having identified a time  $t_0$  at which the BY pulse and its “pseudo-kick” are finished, we remove this effect by beginning the integration of (5) from that point.

## V. RESULTS

We group our simulations into three categories. First we consider the effect of unequal masses alone, where the kick experienced should be along the line connecting the holes. We then add spins to holes of equal horizon mass, to explore the dependence of kicks on pure spin anisotropy; this configuration should yield kicks orthogonal to the line connecting the holes. Finally we consider the combination of both spin and unequal masses, to explore the interrelation of the two mechanisms generating kicks.

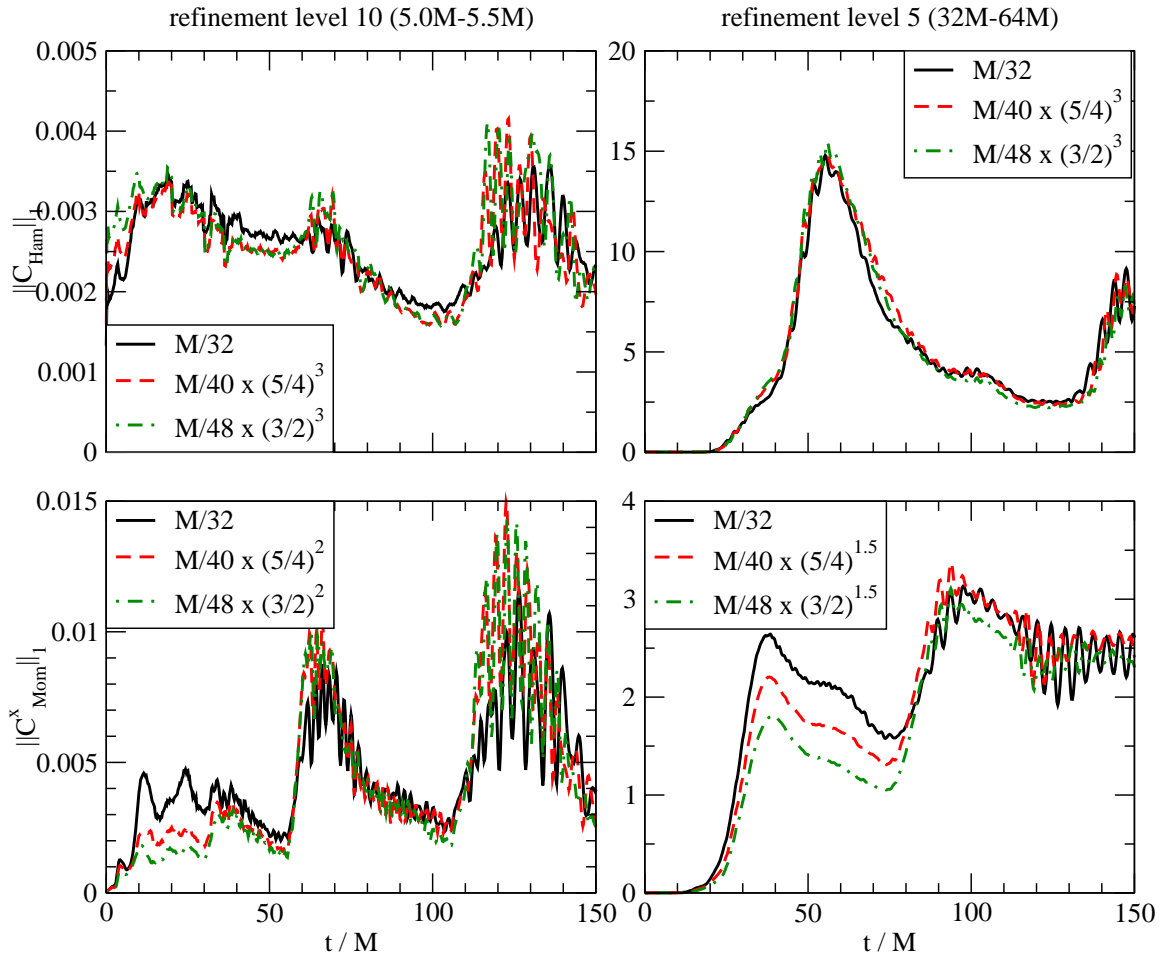


FIG. 1: L1-norm convergence of Hamiltonian (top) and momentum ( $x$  component; bottom) constraints for the  $\text{EQ}_{+-}$  run, in two regions of the simulation grid: just outside the horizons (left), and in the primary radiation extraction region (right). The Hamiltonian constraint displays third-order convergence in both regions, while the momentum constraint convergence drops to 1.5-order in the extraction region.

### A. Unequal masses without spin

The head-on collision of two holes of unequal masses has been considered several times in the past, both with close-limit analysis (CLA) [71] and with fully numerical evolutions in 2D [72]. The CLA results (performed with Misner two-sheeted data) provide a definite prediction of preferential radiation of linear momentum; the numerical results seemed to confirm this, and indicated where the CLA fails. The numerical results were for proper separations far less than ours; extrapolating their results to the larger separations we treat here indicates that a longitudinal kick  $\sim 10\text{km/s}$  would be produced.

In Fig. 5, we plot the  $y$ -component of the thrust  $d\vec{P}/dt$  from Eq. (5), and its time integral from the  $\text{NE}_{00}$  run. Note that the  $x$  and  $z$  components of  $d\vec{P}/dt$  are zero by symmetry: the kick is longitudinal, i.e. along the axis of collision ( $y$  axis). The final kick velocity, given in Table III, is  $\sim 2.7\text{km/s}$ .

The final kick obtained from Fig. 5 is highly consistent across extraction radii, with a spread between the  $R_{\text{ext}} = 30M$  and  $R_{\text{ext}} = 40M$  values of  $\sim 0.5\%$ . We note however that the difference between  $R_{\text{ext}} = 50M$  and  $R_{\text{ext}} = 60M$  is larger than that between  $R_{\text{ext}} = 40M$  and  $R_{\text{ext}} = 50M$ . This appears to be because the extraction surface at  $R_{\text{ext}} = 60M$  lies in a region of less grid refinement than the three closer surfaces.

### B. Equal masses with spin

We now turn to simulations of spinning black holes. We ran two configurations ( $\text{EQ}_{+0}, \text{EQ}_{+-}$ ), as indicated in Table I. As only one particle is spinning in the former case, we should see only “spin-orbit” effects between that spin and the motion of the particle. In the latter case, with two spins, we might also see “spin-spin” ef-



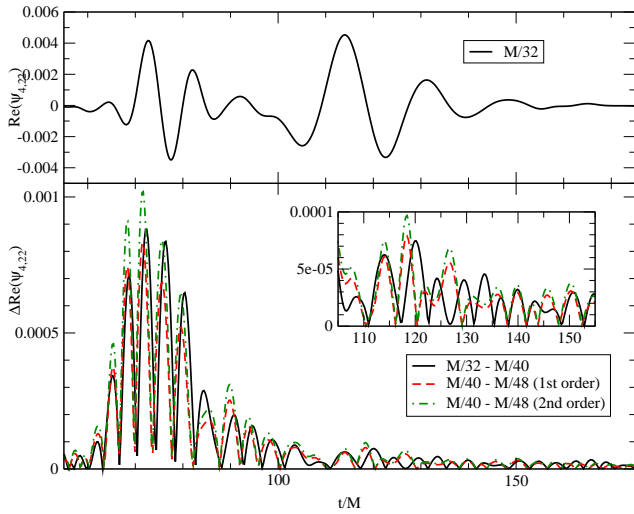


FIG. 2: Convergence of  $\text{Re}(\psi_4)$ , the real part of the dominant  $(2, 2)$  mode of the waveform for the  $\text{EQ}_{+-}$  run. The upper panel shows the thrust for central resolution  $M/32$ , extracted at  $R_{\text{ext}} = 60M$ ; the lower panel shows the absolute differences  $M/32 - M/40$  (solid line) and  $M/40 - M/48$ , the latter scaled to compare with coarse-medium for 1st- and 2nd-order convergence. The inset focuses on the physical part of the waveform, which shows much smaller resolution errors.

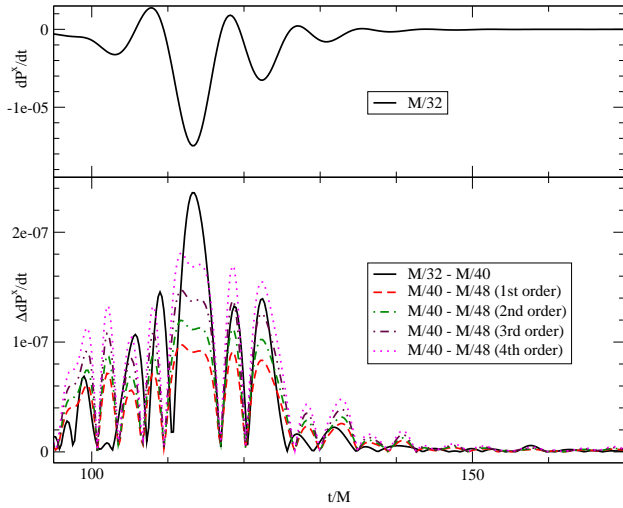


FIG. 3: Convergence of transverse momentum thrust  $dP^x/dt$  for the  $\text{EQ}_{+-}$  run. The upper panel shows the thrust for central resolution  $M/32$ , extracted at  $R_{\text{ext}} = 60M$ ; the lower panel shows the absolute differences  $M/32 - M/40$  (solid line) and  $M/40 - M/48$ , the latter scaled to compare with coarse-medium for 1st- and 2nd-order convergence.

fects; however PN predictions for the latter are of higher

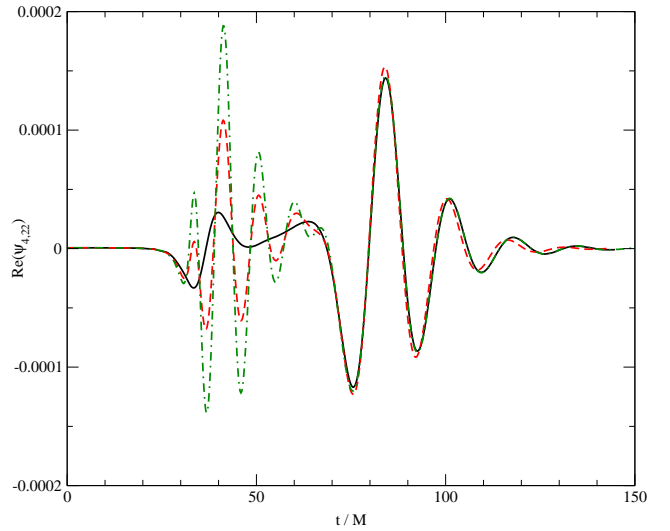


FIG. 4: Dominant  $(l = 2, m = 2)$  mode of the waveform  $\psi_4$  for the three equal-mass configurations:  $\text{EQ}_{00}$  (solid/black),  $\text{EQ}_{+0}$  (dashed/red), and  $\text{EQ}_{+-}$  (dot-dashed/green). These data were extracted at coordinate distance  $R_{\text{ext}} = 30M$ .

PN order than for spin-orbit [73]<sup>1</sup>

In Fig. 6 we show the transverse kick  $\Delta P^x$  observed for both equal-mass data sets. We note that the magnitude of both the BY pulse and the final kick for the  $\text{EQ}_{+-}$  data are roughly double those for  $\text{EQ}_{+0}$  (see Table III). This indicates that the total kick is close to a simple sum of the individual kicks. Thus any spin-spin contribution to the total kick is negligible in comparison to the spin-orbit term.

### C. Unequal masses with spin

Having considered collisions between non-equal mass and non-spinning black holes and equal mass and spinning black holes, we combine both spin and mass ratio in a few cases, the  $\text{NE}_{+-}$ ,  $\text{NEa}_{+-}$ , and  $\text{NEb}_{+-}$  runs.

We show in the upper panel of Fig. 7 the thrust for the  $\text{NE}_{+-}$  case. We note that unlike the simpler cases before,

<sup>1</sup> For the  $\text{EQ}_{+0}$  run presented here, we have used slightly different choices in our numerical evolution: advection terms employed a third-order upwinding scheme, guardcell-filling was fourth-order-accurate, time stepping was performed with a second-order Crank-Nicholson method, no dissipation was used, and the initial lapse function shape was  $\alpha_{\text{init}} = \psi_{BL}^{-2}$ , as in the evolutions of [32]. For this data alone, the physical outer boundary was at  $128M$ , but the outermost extraction here was at  $R_{\text{ext}} = 30M$ . From direct comparison of the thrusts obtained from the two evolution schemes for the  $\text{EQ}_{+-}$  data, we have determined that the only measurable difference is a gauge-driven  $1M$  delay in the arrival of wavefronts at the extraction sphere.

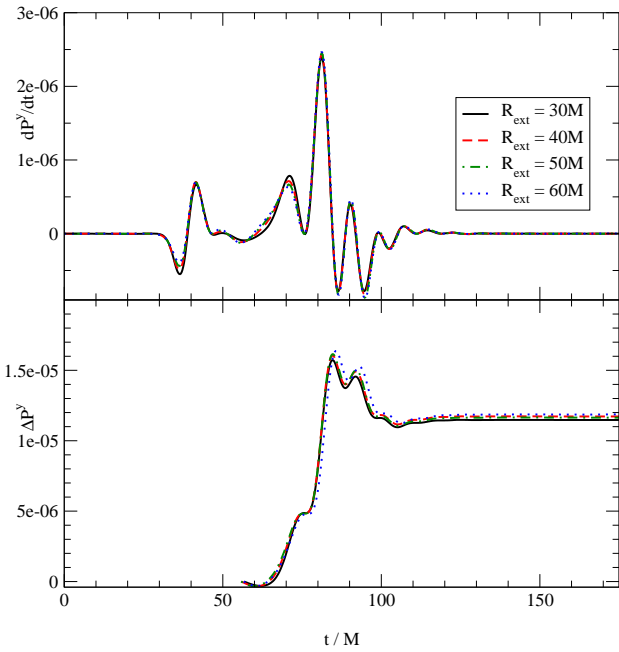


FIG. 5: Longitudinal thrust  $dP^y/dt$  (top) and kick  $\Delta P^y$  (bottom) for  $\text{NE}_{00}$ , at extraction radii  $R_{\text{ext}}$  of  $30M$ ,  $40M$ ,  $50M$  and  $60M$ , where the latter three have been time-shifted by  $10.6M$ ,  $21.0M$  and  $31.4M$ , respectively, to align the highest thrust peak with the  $30M$  case (consistent with time-shift formula Eq. (14) in [67]).

the BY pulse and physical signal are *not* obviously separated in the thrust. As a result, we may expect to have trouble determining where to begin the kick integrations.

In principle, a larger initial separation would mean more time between the BY pulse – emitted at  $t = 0$  and lasting  $\sim 43M$  (see discussion in Section IV A) – and the bulk of the physical radiation, which only becomes large near merger. The main physical kick will certainly be different in magnitude between the two cases, and even the BY pulse magnitude may differ, depending on the dependence of the spectrum on the initial separation of the binary. Nevertheless, we *can* expect the BY pulse *duration* to be the same, as this is determined by the leading quasinormal frequencies of each hole, and these frequencies are fully determined by the mass and spin of each hole, which is a constant between the two cases. In Fig. 7, we show  $dP^x/dt$  and  $\Delta P^x$  for  $\text{NE}_{+-}$ , with a coordinate separation of  $8M$ , and  $\text{NEa}_{+-}$ , with a coordinate separation of  $12M$ .

The extra initial separation ( $\text{NEa}_{+-}$ ) leads to a very similar physical thrust, delayed  $\sim 22M$  relative to the original separation ( $\text{NE}_{+-}$ ). This physical thrust begins at  $\sim 114M$  for the detector at  $R_{\text{ext}} = 60M$ . Integrating forward from any time up to  $\sim 20M$  before this will result in the same transverse kick for the  $\text{NEa}_{+-}$  case. To ensure that as much of the physical kick as possible is obtained in the smaller-separation case, we integrate

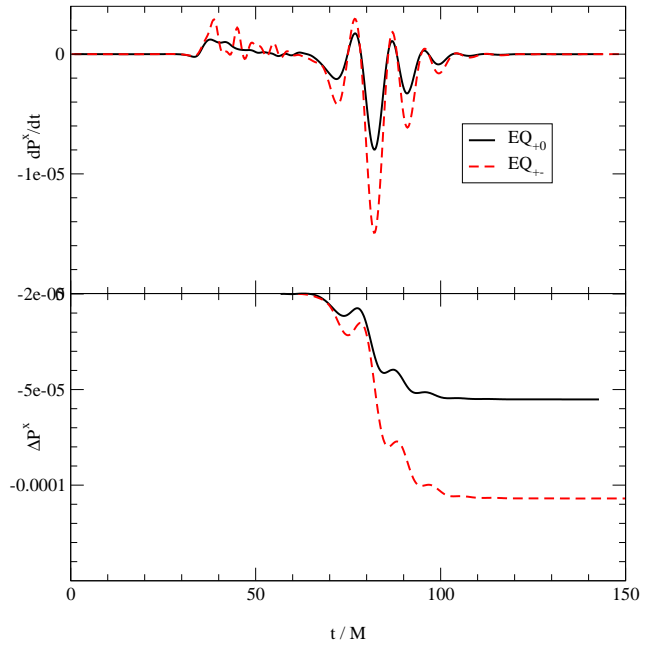


FIG. 6: Transverse thrust  $dP^x/dt$  and kick  $\Delta P^x$  for the spinning, equal-mass cases  $\text{EQ}_{+0}$  (black/solid) and  $\text{EQ}_{+-}$  (red/dashed), at extraction radii  $R_{\text{ext}}$  of  $30M$ , where the  $\text{EQ}_{+-}$  data have been time-shifted by  $1M$  to compensate for gauge differences.

the  $\text{NE}_{+-}$  thrust from  $t_0 = 114M - 22M = 92M$  at  $R_{\text{ext}} = 60M$ .

In Figs. 8 and 9 we present the momentum kicks in the transverse ( $x$ ) and longitudinal ( $y$ ) directions for the  $\text{NE}_{+-}$  data set, comparing with the kicks seen from the  $\text{NE}_{00}$  and  $\text{EQ}_{+-}$  cases before.

Taking the transverse direction first, we see from Fig. 8 that the momentum kick from  $\text{NE}_{+-}$  is significantly *smaller* than that of  $\text{EQ}_{+-}$ . The spin angular momentum  $S$  present in each case is the same, indicating that the kick is not a function of  $S$ . In contrast, the momentum kick observed from  $\text{NEb}_{+-}$  is much larger.

The physical momentum kicks from these runs are presented in Table III. We note that the ratio of transverse momentum kicks  $\Delta P^x$  between the cases  $\text{NE}_{+-}$  and  $\text{NEb}_{+-}$  is roughly  $2/3$ , consistent with the PN-derived ratio (see Eq. (8) below).

In addition to finite differencing inaccuracy, for these cases we find that the high slope in the thrust for these cases yields a non-negligible error associated with the choice in integration starting point  $t_0$ . As before, we assess a timing-related error by integrating the thrust from  $t_0$  and from  $t_0 \pm 5M$ . The resulting central kicks and errors are given in Table III.

With this in mind, we turn to the longitudinal direction. Here we see that the initial BY burst is comparable in magnitude to the physical later part. Using for

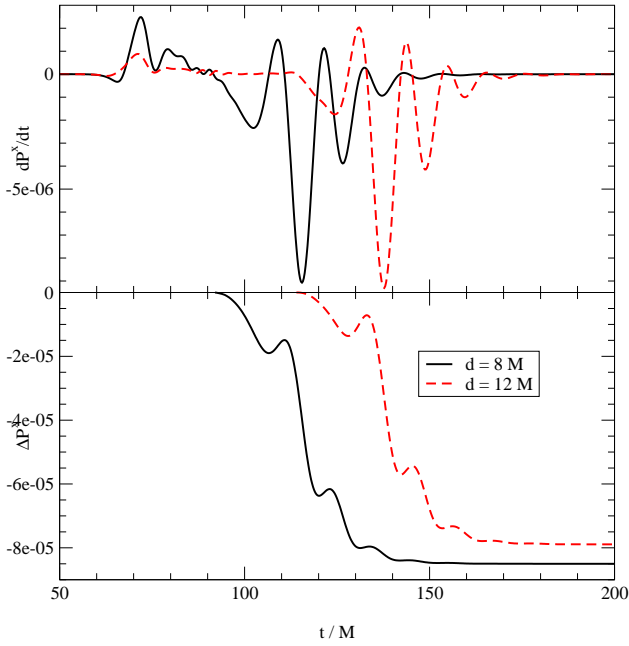


FIG. 7: Transverse thrust  $dP^x/dt$  (top) and kick  $\Delta P^x$  (bottom) for unequal-mass-with-spin data, at coordinate separations  $8M$  ( $NE_{+-}$ ; black/solid) and  $12M$  ( $NE_{a+-}$ ; red/dashed). These data were extracted at  $R_{\text{ext}} = 60M$ .

consistency the same integration starting time as in the transverse direction, we present the longitudinal kicks in Table III. It is clear that the  $t_0$  uncertainty leads to large relative errors for the longitudinal kicks. To this uncertainty, all longitudinal kicks are consistent with the zero-spin case,  $NE_{00}$ .

#### D. Summary of Results

We draw together in Table III the kicks observed in each of our simulations. We can develop some expectations for the comparative results by referencing post-Newtonian theory estimates of the radiative linear momentum loss due to unequal masses and spin-orbit coupling. For example, adapting Eqs. (3.31a-b) of [73] to radial infall along the  $y$  axis, we find:

$$\dot{\vec{P}}_N = \frac{16}{105} \frac{\delta m}{m_T} \nu^2 \left( \frac{m_T}{r} \right)^4 \dot{r} \left( -\dot{r}^2 + \frac{2m_T}{r} \right) \hat{e}_y, \quad (7)$$

$$\dot{\vec{P}}_{SO} = -\frac{16}{15} \frac{\nu^2 \dot{r}^2}{r} \left( \frac{m_T}{r} \right)^4 (a_1 + a_2) \hat{e}_x, \quad (8)$$

where  $m_T = m_1 + m_2$ ,  $\delta m = m_1 - m_2$ , and  $r$  is the spatial separation of the two particles, with  $\dot{r} < 0$ .

In studies of spin such as the one carried out here, whether physical effects scale with angular momentum

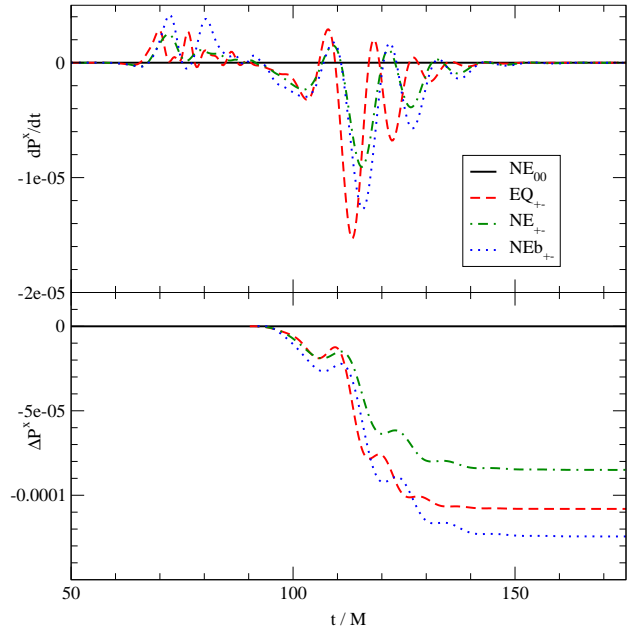


FIG. 8: Transverse thrust  $dP^x/dt$  (top) and kick  $\Delta P^x$  (bottom) for  $NE_{00}$  (black),  $EQ_{+-}$  (red), and  $NE_{+-}$  (green), and  $NE_{b+-}$  (blue). These data were extracted at  $R_{\text{ext}} = 60M$ .

$S$ , the Kerr parameter  $a \equiv S/m$  or the dimensionless number  $a/m$  is an open question. The post-Newtonian result of Eq. (8) predicts a thrust (and hence kick) that scales with  $a$  for each hole. We have tried to address this uncertainty in our choice of data sets.

It is informative to compare the transverse kick results from each of our spinning data sets with each other, in light of post-Newtonian predictions. Looking at Eq. (8), we assume that the right-hand side is more or less insensitive to the details of the rate of infall, the important length scale then being the total mass  $m_T$  of the binary. With this in mind, the remaining freedom lies in the spin scaling  $(a_1 + a_2)/m_T$ . Relative to the  $EQ_{+-}$  case, this scaling factor is  $\{1/2, 2/3, 2/3, 1\}$  for cases  $\{EQ_{+0}, NE_{+-}, NE_{a+-}, NE_{b+-}\}$ . In Fig. 10 we combine the post-BY-pulse part of the transverse thrust  $dP^x/dt$  of each case, with times rescaled according to the ADM mass from Table I, and translated so that the peaks coincide. We have also rescaled the thrust amplitude by the factors appropriate to the PN above. Surprisingly, after this rescaling, the five thrusts fit very well, with a deviation of overall amplitude of  $\sim 20\%$ . This appears to indicate that PN predictions of recoil kicks have validity further into the merger regime than would be expected.

We have looked at the puncture tracks of the holes, which give a coordinate speed estimate for the final hole. These agree with the radiation-generated kick in order-of-magnitude and relative scaling (transverse vs longitudinal velocity components), but not in detail; in partic-



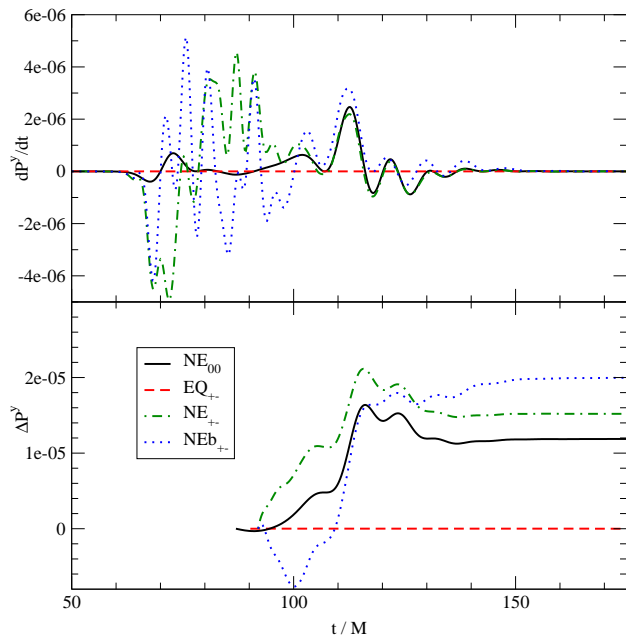


FIG. 9: Longitudinal thrust  $dP^y/dt$  (top) and kick  $\Delta P^y$  (bottom) for  $NE_{00}$  (black),  $EQ_{+-}$  (red), and  $NE_{+-}$  (green), and  $NEb_{+-}$  (blue). These data were extracted at  $R_{\text{ext}} = 60 M$ .

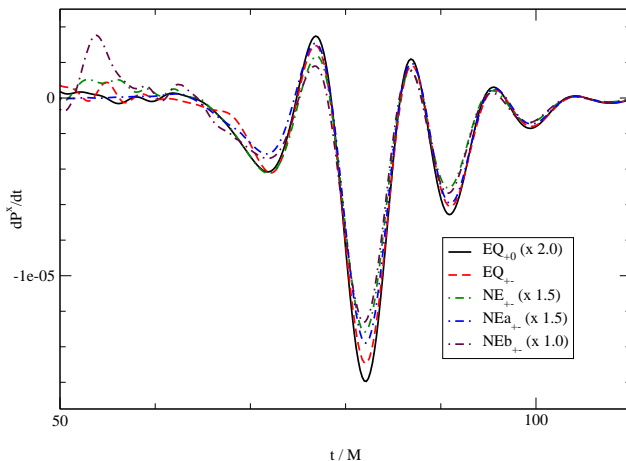


FIG. 10: Transverse thrust  $dP^x/dt$  for all spinning data sets:  $EQ_{+0}$ ,  $EQ_{+-}$ ,  $NE_{+-}$ ,  $NEa_{+-}$ , and  $NEb_{+-}$ . Time has been rescaled by the ADM mass for each data set, and translated relative to  $EQ_{+-}$  to line up peaks. Amplitudes have been scaled relative to  $EQ_{+-}$  according to PN predictions. These data were extracted at  $R_{\text{ext}} = 30 M$ .

## VI. DISCUSSION

In this paper, we have addressed the roles of unequal masses and spins in producing recoil kicks in head-on col-

lisions. We have chosen sample spins and mass ratios to explore how important spin effects are for kicks, and how

ular, we do not see a velocity plateau; given the small recoil velocities (compared to inspiral) in question here, the puncture-derived position may just not be accurate enough. It should be borne in mind also that the puncture track is highly coordinate-dependent, and has no guaranteed relationship to physical quantities such as the kick.

We also present in Table IV estimates for the final Kerr parameters  $M_f$  and  $a_f$  of the post-merger hole for each simulation. We calculate these estimates in two different ways: First, we compare the initial ADM energy and angular momentum of the system with the radiated energy and angular momentum. In this we are limited by the accuracy of the ADM energy, reliable to three significant digits. Second, we use the  $(2, 2)$  mode of the radiation after the final amplitude peak to extract a quasinormal-mode frequency and damping time, and hence to determine the underlying Kerr parameters, assuming the perturbative limit. This latter method is sensitive to the determination of an appropriate starting time for the QNM fit, as well as the neglect of QNM overtones. The determination  $a/M = 0.0252$  for the  $NE_{00}$  data set, which can contain *no* angular momentum, indicates the level of error of this method.

TABLE III: Final integrated momentum kicks and corresponding kick velocities. In each case, we have removed “BY pulse” effects through deferring integration until after the passage of the pulse. Quoted errors at each extraction radius are obtained by varying the integration starting time by  $\pm 5M$ .

Run	$t_0$ ( $M$ )	$\Delta P^x$ ( $10^{-5}$ )	$\Delta P^y$ ( $10^{-5}$ )	$v_x$ (km/s)	$v_y$ (km/s)	$v$ (km/s)
NE <sub>00</sub> 30M	51.0	0.0	$1.12 \pm 0.02$	0.0	$2.71 \pm 0.05$	$2.71 \pm 0.05$
40M	61.7	0.0	$1.14 \pm 0.04$	0.0	$2.76 \pm 0.10$	$2.76 \pm 0.10$
60M	82.9	0.0	$1.16 \pm 0.04$	0.0	$2.81 \pm 0.10$	$2.81 \pm 0.10$
EQ <sub>+0</sub> 20M	46.1	$-5.13 \pm 0.04$	0.0	$-15.38 \pm 0.12$	0.0	$15.38 \pm 0.12$
30M	56.6	$-5.51 \pm 0.01$	0.0	$-16.52 \pm 0.03$	0.0	$16.52 \pm 0.03$
EQ <sub>+−</sub> 30M	59.6	$-10.70 \pm 0.08$	0.0	$-32.08 \pm 0.24$	0.0	$32.08 \pm 0.24$
40M	70.0	$-10.53 \pm 0.09$	0.0	$-31.57 \pm 0.27$	0.0	$31.57 \pm 0.27$
60M	90.5	$-10.81 \pm 0.15$	0.0	$-32.41 \pm 0.45$	0.0	$32.41 \pm 0.45$
NE <sub>+-</sub> 40M	72.0	$-8.47 \pm 0.31$	$1.36 \pm 1.10$	$-20.41 \pm 0.75$	$3.28 \pm 2.65$	$20.67 \pm 0.85$
60M	92.0	$-8.50 \pm 0.27$	$1.52 \pm 1.36$	$-20.48 \pm 0.67$	$3.66 \pm 3.28$	$20.80 \pm 0.88$
NEa <sub>+-</sub> 40M	94.0	$-7.89 \pm 0.26$	$1.04 \pm 0.08$	$-18.92 \pm 0.63$	$2.49 \pm 0.20$	$19.08 \pm 0.63$
60M	114.0	$-7.89 \pm 0.21$	$1.00 \pm 0.07$	$-18.92 \pm 0.51$	$2.40 \pm 0.17$	$19.07 \pm 0.51$
NEb <sub>+-</sub> 40M	72.0	$-12.33 \pm 0.56$	$2.03 \pm 0.64$	$-29.41 \pm 1.34$	$4.84 \pm 1.53$	$29.81 \pm 1.35$
60M	92.0	$-12.44 \pm 0.39$	$2.00 \pm 0.55$	$-29.67 \pm 0.93$	$4.77 \pm 1.31$	$30.05 \pm 0.94$

TABLE IV: Basic parameters  $M_f$  and  $a_f$  of the post-merger hole, as calculated from radiated energy and angular momentum (“rad”), and from measured quasi-normal mode frequencies (“QNM”). All quantities based on extraction at  $R_{\text{ext}} = 60M$ , except for  $R_{\text{ext}} = 30M$  for run EQ<sub>+0</sub>.

Run	$M_{ADM}/M$	$E_{\text{rad}}/M$	$M_{f,\text{rad}}/M$	$J_{ADM}/M^2$	$J_{\text{rad}}/M^2$	$(J/M^2)_{f,\text{rad}}$	$M_{f,QNM}/M$	$(a/M)_{f,QNM}$
NE <sub>00</sub>	1.24	$-6.14 \times 10^{-4}$	1.24	0.0	0.0	0.0	1.2536	0.0252
EQ <sub>+0</sub>	1.00	$-7.90 \times 10^{-4}$	1.00	0.2	$-1.101 \times 10^{-3}$	0.1992	1.0102	0.3507
EQ <sub>+−</sub>	1.00	$-9.02 \times 10^{-4}$	1.00	0.0	$-0.000 \times 10^{-4}$	0.0	1.0113	0.0198
NE <sub>+-</sub>	1.24	$-8.19 \times 10^{-4}$	1.24	0.0	$-3.508 \times 10^{-4}$	$2.33 \times 10^{-4}$	1.2585	0.0261
NEa <sub>+-</sub>	1.25	$-8.16 \times 10^{-4}$	1.25	0.0	$-1.582 \times 10^{-4}$	$1.01 \times 10^{-4}$	1.2676	0.0300
NEb <sub>+-</sub>	1.26	$-1.10 \times 10^{-3}$	1.26	0.2486	$-5.000 \times 10^{-4}$	0.154	1.2582	0.2175

the effects of spin and mass ratio are related in generating kicks. We have carried out kick extractions from data sets with mass ratios of 1 and 2/3, and with spins on one or both holes.

We have observed that head-on collisions of spinning black holes can produce significant kicks. For the anti-aligned spin cases we have studied, the spin-kicks are transverse to the direction of initial separation. The magnitude of the kicks, and even the thrust curves (Fig. 10), scale with the sum of the individual black hole spin parameters,  $a_1 + a_2$ . These kicks easily exceed the longitudinal kick produced in the case of unequal masses. To the accuracy available in our simulations, we find that the kicks due to the mass ratio and spins are indeed orthogonal and independent. Both the spin scaling and the orthogonality of spin-kicks and mass-ratio-kicks are consistent with leading-order PN predictions for these effects, as given by Eqs. (7,8).

It is remarkable that the PN predictions seem to describe our results. The kick-producing radiation derived

in our simulations is generated in the systems’ non-linear mergers and ringdowns, where the assumptions behind the PN approximations clearly do not apply. In general terms, the PN analysis (see [73]) provides that the unequal-mass-kick is produced by a coupling of the mass-quadrupole and mass-octupole moments, while the spin-kick is produced by a coupling of the mass-quadrupole and current-quadrupole moments. At least heuristically, we can consider these moments even in the nonlinear problem. In our problem, the presence of spin does not seem to have a large effect on the mass moments, as is suggested by the spin-independence of the mass-quadrupole-dominated ( $l = 2, m = 2$ ) waveforms, seen in Fig.4. The leading effect of putting spin on the black holes is to scale up the current-quadrupole moment. For general spins, this term scales with  $(\tilde{S}_1/m_1 - \tilde{S}_2/m_2)$ .

In the more important case of inspiraling black holes, our results suggest that the current-quadrupole effects should also provide strong kicks, scaling in a similar way with spin. Because of the scaling with  $S/m$  we would

generally expect the strongest spin-kicks for nearly-equal-mass mergers. Our results support the use of PN expressions (as in [39, 41, 42]) to predict the scaling of spin-kicks for black hole configurations that have not yet been studied.

Since initial submission of this paper, several groups have begun mode-based analysis of recoil kicks from binary inspiral [74, 75]. Additionally, further investigation of the maximum size and genericity of spin superkicks has been undertaken [76, 77, 78, 79]. These substantial predictions have opened the door to exciting new possibilities in the astronomy of supermassive black holes and galactic nuclei.

### Acknowledgments

We would like to thank Sean McWilliams for useful discussions and insight.

This work was supported in part by NASA grants O5-BEFS-05-0044 and 06-BEFS06-19. The simulations were carried out using Project Columbia at NASA Ames Research Center and at the NASA Center for Computational Sciences at Goddard Space Flight Center. D.C. was supported in part by The Korea Research Foundation and The Korean Federation of Science and Technology Societies Grant funded by Korea Government (MOEHRD, Basic Research Promotion Fund). B.K. was supported by the Research Associateship Programs Office of the National Research Council and the NASA Postdoctoral Program at the Oak Ridge Associated Universities.

The PARAMESH software used in this work was developed at the NASA Goddard Space Flight Center and Drexel University under NASA's HPCC and ESTO/CT projects and under grant NNG04GP79G from the NASA/AISR project.

- 
- [1] D. Merritt, M. Milosavljevic, M. Favata, S. A. Hughes, and D. E. Holz, *Astrophys. J.* **607**, L9 (2004), arXiv:astro-ph/0402057.
  - [2] M. Boylan-Kolchin, C.-P. Ma, and E. Quataert, *Astrophys. J.* **613**, L37 (2004), arXiv:astro-ph/0407488.
  - [3] Z. Haiman, *Astrophys. J.* **613**, 36 (2004), arXiv:astro-ph/0404196.
  - [4] P. Madau and E. Quataert, *Astrophys. J.* **606**, L17 (2004), arXiv:astro-ph/0403295.
  - [5] J. Yoo and J. Miralda-Escudé, *Astrophys. J.* **614**, L25 (2004), arXiv:astro-ph/0406217.
  - [6] M. Volonteri and R. Perna, *Mon. Not. Roy. Astron. Soc.* **358**, 913 (2005), arXiv:astro-ph/0501345.
  - [7] N. I. Libeskind, S. Cole, C. S. Frenk, and J. C. Helly, *Mon. Not. Roy. Astron. Soc.* **368**, 1381 (2006), arXiv:astro-ph/0512073.
  - [8] M. Micic, T. Abel, and S. Sigurdsson, *Mon. Not. R. Astron. Soc.* **372**, 1540 (2006), arXiv:astro-ph/0609443.
  - [9] M. C. Miller and D. P. Hamilton, *Mon. Not. R. Astron. Soc.* **330**, 232 (2002), arXiv:astro-ph/0106188.
  - [10] H. Mouri and Y. Taniguchi, *Astrophys. J.* **580**, 844 (2002), arXiv:astro-ph/0208053.
  - [11] M. C. Miller and E. J. M. Colbert, *Int. J. Mod. Phys. D* **13**, 1 (2004), arXiv:astro-ph/0308402.
  - [12] K. Gültekin, M. C. Miller, and D. P. Hamilton, *Astrophys. J.* **616**, 221 (2004), arXiv:astro-ph/0402532.
  - [13] K. Gültekin, M. Coleman Miller, and D. P. Hamilton, *Astrophys. J.* **640**, 156 (2006), arXiv:astro-ph/0509885.
  - [14] R. M. O'Leary, F. A. Rasio, J. M. Fregeau, N. Ivanova, and R. O'Shaughnessy, *Astrophys. J.* **637**, 937 (2006), arXiv:astro-ph/0508224.
  - [15] M. C. Miller and D. P. Hamilton, *Astrophys. J.* **576**, 894 (2002), arXiv:astro-ph/0202298.
  - [16] A. Sesana, F. Haardt, P. Madau, and M. Volonteri, *Astrophys. J.* **623**, 23 (2005), arXiv:astro-ph/0409255.
  - [17] A. Peres, *Phys. Rev.* **128**, 2471 (1962).
  - [18] J. D. Bekenstein, *Astrophys. J.* **183**, 657 (1973).
  - [19] M. J. Fitchett, *Mon. Not. R. Astron. Soc.* **203**, 1049 (1983).
  - [20] M. J. Fitchett and S. Detweiler, *Mon. Not. R. Astron. Soc.* **211**, 933 (1984).
  - [21] I. H. Redmount and M. J. Rees, *Comments Astrophys.* **14**, 165 (1989).
  - [22] A. G. Wiseman, *Phys. Rev. D* **46**, 1517 (1992).
  - [23] M. Favata, S. A. Hughes, and D. E. Holz, *Astrophys. J.* **607**, L5 (2004), arXiv:astro-ph/0402056.
  - [24] L. Blanchet, M. S. S. Qusailah, and C. M. Will, *Astrophys. J.* **635**, 508 (2005), arXiv:astro-ph/0507692.
  - [25] T. Damour and A. Gopakumar, *Phys. Rev. D* **73**, 124006 (2006), arXiv:gr-qc/0602117.
  - [26] F. Pretorius, *Phys. Rev. Lett.* **95**, 121101 (2005), arXiv:gr-qc/0507014.
  - [27] M. Campanelli, C. O. Lousto, P. Marronetti, and Y. Zlochower, *Phys. Rev. Lett.* **96**, 111101 (2006), arXiv:gr-qc/0511048.
  - [28] J. G. Baker, J. Centrella, D.-I. Choi, M. Koppitz, and J. van Meter, *Phys. Rev. Lett.* **96**, 111102 (2006), arXiv:gr-qc/0511103.
  - [29] M. Campanelli, C. O. Lousto, and Y. Zlochower, *Phys. Rev. D* **73**, 061501(R) (2006), arXiv:gr-qc/0601091.
  - [30] J. G. Baker, J. Centrella, D.-I. Choi, M. Koppitz, and J. van Meter, *Phys. Rev. D* **73**, 104002 (2006), arXiv:gr-qc/0602026.
  - [31] A. Buonanno, G. B. Cook, and F. Pretorius, *Phys. Rev. D* **75**, 124018 (2007), arXiv:gr-qc/0610122.
  - [32] J. G. Baker, S. T. McWilliams, J. R. van Meter, J. Centrella, D.-I. Choi, B. J. Kelly, and M. Koppitz, *Phys. Rev. D* **75**, 124024 (2007), arXiv:gr-qc/0612117.
  - [33] F. Herrmann, D. Shoemaker, and P. Laguna, *Class. Quantum Grav.* **24**, S33 (2007), arXiv:gr-qc/0601026.
  - [34] J. G. Baker, J. Centrella, D.-I. Choi, M. Koppitz, J. van Meter, and M. C. Miller, *Astrophys. J.* **653**, L93 (2006), arXiv:astro-ph/0603204.
  - [35] J. A. Gonzalez, U. Sperhake, B. Brügmann, M. Han-

- nam, and S. Husa, Phys. Rev. Lett. **98**, 091101 (2007), arXiv:gr-qc/0610154.
- [36] M. Campanelli, C. O. Lousto, and Y. Zlochower, Phys. Rev. D **74**, 041501(R) (2006), arXiv:gr-qc/0604012.
- [37] M. Campanelli, C. O. Lousto, and Y. Zlochower, Phys. Rev. D **74**, 084023 (2006), arXiv:astro-ph/0608275.
- [38] M. Campanelli, C. O. Lousto, Y. Zlochower, B. Krishnan, and D. Merritt, Phys. Rev. D **75**, 064030 (2007), arXiv:gr-qc/0612076.
- [39] F. Herrmann, I. Hinder, D. Shoemaker, P. Laguna, and R. A. Matzner, Astrophys. J. **661**, 430 (2007), arXiv:gr-qc/0701143.
- [40] M. Koppitz, D. Pollney, C. Reisswig, L. Rezzolla, J. Thornburg, P. Diener, and E. Schnetter, Phys. Rev. Lett. **99**, 041102 (2007), arXiv:gr-qc/0701163.
- [41] J. G. Baker, W. D. Boggs, J. Centrella, B. J. Kelly, S. T. McWilliams, M. C. Miller, and J. R. van Meter, Astrophys. J. **668**, 1140 (2007), arXiv:astro-ph/0702390.
- [42] M. Campanelli, C. O. Lousto, Y. Zlochower, and D. Merritt, Astrophys. J. **659**, L5 (2007), arXiv:gr-qc/0701164.
- [43] J. A. Gonzalez, M. D. Hannam, U. Sperhake, B. Brügmann, and S. Husa, Phys. Rev. Lett. **98**, 231101 (2007), arXiv:gr-qc/0702052.
- [44] J. R. van Meter, J. G. Baker, M. Koppitz, and D.-I. Choi, Phys. Rev. D **73**, 124011 (2006), arXiv:gr-qc/0605030.
- [45] M. Hannam, S. Husa, D. Pollney, B. Brügmann, and N. Ó Murchadha (2006), arXiv:gr-qc/0606099.
- [46] B. Brügmann, J. A. Gonzalez, M. Hannam, S. Husa, U. Sperhake, and W. Tichy (2006), arXiv:gr-qc/0610128.
- [47] U. Sperhake, Phys. Rev. D **76**, 104015 (2007), arXiv:gr-qc/0606079.
- [48] S. Brandt and B. Brügmann, Phys. Rev. Lett. **78**, 3606 (1997), arXiv:gr-qc/9703066.
- [49] J. D. Brown and L. L. Lowe, J. Comput. Phys. **209**, 582 (2005), arXiv:gr-qc/0411112.
- [50] J. M. Bowen and J. W. York, Phys. Rev. D **21**, 2047 (1980).
- [51] N. Ó Murchadha and J. York, Phys. Rev. D **10**, 2345 (1974).
- [52] D. Christodoulou, Phys. Rev. Lett. **25**, 1596 (1970).
- [53] J. Thornburg, Class. Quantum Grav. **21**, 743 (2004), AIP Conf. Proceedings, v. 686, pp. 247-252, (2003), arXiv:gr-qc/0306056.
- [54] S. Dain, C. O. Lousto, and R. Takahashi, Phys. Rev. D **65**, 104038 (2002), arXiv:gr-qc/0201062.
- [55] T. W. Baumgarte and S. L. Shapiro, Phys. Rev. D **59**, 024007 (1998), arXiv:gr-qc/9810065.
- [56] M. Shibata and T. Nakamura, Phys. Rev. D **52**, 5428 (1995).
- [57] P. Hübner, Class. Quantum Grav. **16**, 2823 (1999).
- [58] M. D. Duez, S. L. Shapiro, and H.-J. Yo, Phys. Rev. D **69**, 104016 (2004), arXiv:gr-qc/0401076.
- [59] P. MacNeice, K. Olson, C. Mobarry, R. de Fainchtein, and C. Packer, Computer Physics Comm. **126**, 330 (2000).
- [60] K. Olson and P. MacNeice, in *Adaptive Mesh Refinement-Theory and Applications, Proceedings of the Chicago Workshop on Adaptive Mesh Refinement Methods, Series: Lecture Notes in Computational Science and Engineering*, edited by T. Plewa, T. Linde, and G. Weirs (Springer, Berlin, 2005), vol. 41.
- [61] K. Olson, in *Parallel Computational Fluid Dynamics 2005: Theory and Applications: Proceedings of the Parallel CFD Conference, College Park, MD, U.S.A.*, edited by A. Deane, A. Ecer, G. Brenner, D. Emerson, J. McDonough, J. Periaux, N. Satofuka, and D. Tromeur-Dervout (Elsevier, 2006).
- [62] [http://www.physics.drexel.edu/~olson/paramesh-doc/Users\\_manual](http://www.physics.drexel.edu/~olson/paramesh-doc/Users_manual)
- [63] B. Imbiriba et al., Phys. Rev. D **70**, 124025 (2004), arXiv:gr-qc/0403048.
- [64] L. Lehner, S. L. Liebling, and O. Reula, Class. Quantum Grav. **23**, S421 (2006), arXiv:gr-qc/0510111.
- [65] E. T. Newman and K. P. Tod, in *General Relativity and Gravitation: One hundred years after the birth of Albert Einstein, vol. 2*, edited by A. Held (Plenum Press, NY, 1981), pp. 1-36.
- [66] C. W. Misner, Class. Quantum Grav. **21**, S243 (2004), arXiv:gr-qc/9910044.
- [67] D. R. Fiske, J. G. Baker, J. R. van Meter, D.-I. Choi, and J. M. Centrella, Phys. Rev. D **71**, 104036 (2005), arXiv:gr-qc/0503100.
- [68] J. D. Brown (2007), arXiv:0705.3845 [gr-qc].
- [69] M. Hannam, S. Husa, B. Brügmann, J. A. Gonzalez, and U. Sperhake, Class. Quantum Grav. **24**, S15 (2007), arXiv:gr-qc/0612001.
- [70] E. Berti, V. Cardoso, and C. M. Will, Phys. Rev. D **73**, 064030 (2006), arXiv:gr-qc/0512160.
- [71] Z. Andrade and R. H. Price, Phys. Rev. D **56**, 6336 (1997), arXiv:gr-qc/9611022.
- [72] P. Anninos and S. Brandt, Phys. Rev. Lett. **81**, 508 (1998), arXiv:gr-qc/9806031.
- [73] L. E. Kidder, Phys. Rev. D **52**, 821 (1995), arXiv:gr-qc/9506022.
- [74] J. D. Schnittman, A. Buonanno, J. R. van Meter, J. G. Baker, W. D. Boggs, J. Centrella, B. J. Kelly, and S. T. McWilliams (2007), arXiv:0707.0301 [gr-qc].
- [75] B. Brügmann, J. A. Gonzalez, M. Hannam, S. Husa, and U. Sperhake (2007), arXiv:0707.0135 [gr-qc].
- [76] M. Campanelli, C. O. Lousto, Y. Zlochower, and D. Merritt, Phys. Rev. Lett. **98**, 231102 (2007), arXiv:gr-qc/0702133.
- [77] W. Tichy and P. Marronetti, Phys. Rev. D **76**, 061502(R) (2007), arXiv:gr-qc/0703075.
- [78] F. Herrmann, I. Hinder, D. Shoemaker, P. Laguna, and R. A. Matzner, Phys. Rev. D **76**, 084032 (2007), arXiv:0706.2541 [gr-qc].
- [79] C. O. Lousto and Y. Zlochower (2007), arXiv:0708.4048 [gr-qc].